

Electrolytic Decomposition of Hydroxylammonium Nitrate (HAN) Mixtures in Micropropulsion

T. F. Wahida, Nor Hafizah, Fairul Azmin
Development and Operation Space System Division
National Space Agency (ANGKASA)
Banting, Selangor
farahida@angkasa.gov.my

JK. Chin, Kai Seng Koh
Faculty of Engineering
University of Nottingham, Malaysia Campus (UNMC)
Semenyih, Selangor
Jit-Kai.Chin@nottingham.edu.my

Abstract— Hydroxylammonium Nitrate (HAN) has been considered as a next generation "green" monopropellant candidate because of its excellent good chemical performance but low toxicity, ease of handling and storage and clean post combustion products. In our previous work (Koh et. Al. 2013), large scale electrolytic decomposition of HAN solution has been studied and characterized using commercial copper wire and Aluminium respectively.

In order to utilize the technology in a micropropulsion for future micro-spacecraft or micro-satellite application. A micropropulsion has been designed and fabricated with Poly-Dimethylsiloxane (PDMS) as structural material. The transparent nature of PDMS enables visualization of reactive as structural material. The micropropulsion was fabricated using modified soft-lithography method and bonded to a piece of glass. The device consisted of a HAN mixture reservoir, transport channel as well as a reaction chamber. A pair of commercial copper wire was inserted into the reaction chamber to initiate decomposition of HAN mixture via electrolytic decomposition.

In this paper, Electrolytic decomposition of 73 wt% Hydroxylammonium Nitrate (HAN) solution was successfully demonstrated with DC power 300W in carefully designed transparent PDMS-based micro-combustion chambers. Experimental results show that more vigorous reaction occurred at high inlet flowrate of 50 μ l/min ($Re = 0.88$) in which only 10 - 48% of space inside the micro-combustion chamber occupied by the un-decomposed HAN solution compared to 40 - 62% at inlet flowrate of 10 μ l/min ($Re = 0.18$).

Keywords—*monopropellant; micropropulsion; hydroxylammonium nitrate; microcombustion;*

I. INTRODUCTION

Hydroxylammonium Nitrate (HAN) with the chemical formula NH_3OHNO_3 has been recognized as a liquid gun material and rocket propellant due to its unique advantages such high energy density, low handling and storage cost. The relatively high specific impulse and clean post combustion gas specific gas species has made HAN known to be a great oxidizer for hybrid rockets [1-3]. However, several crucial

challenges, including combustion stability and reliable ignition/combustion method that can provide high energy

output need to be resolved, in order to further develop other potential usage of HAN in various applications ranging from space transport to daily microenergy resources for microreactor [4-5].

Extensive studies relevant to HAN have been conducted including its combustion behavior [6-7], as well s thermal heating or catalytic ignition [8-10]. The process results in huge energy loss from ignition, which is particularly more significant at the microscale due to the large surface to volume ratio of combustion chamber.

II. THEORY OF HAN DECOMPOSITION

Thermal and electrolytic decomposition paths of HAN solution are compared in Table 1. In thermal decomposition water evaporation, which is the chemical rate determining step, will firstly take place, followed by ignition as nitric acid reacts with hydroxylamine. In the decay stage, six simplified kinetic equations occur simultaneously were proposed. The decomposition via electrolysis is similar in ignition and decay stages as HAN thermal decomposition process but the only main difference that makes electrolytic decomposition an improved decomposition technique is the initiation process. Electrolytic decomposition utilities the charge-rich characteristic of HAN solution to initiate decomposition by simulating electrons transfer within HAN solution via electrolysis to reach its excited stage, before further reactions take place as described in previous section.

Table 1. Comparison of reaction mechanisms using different HAN decomposition techniques.

Thermal decomposition		Electrolytic decomposition
Induction: 1. $\text{HAN} + \text{H}_2\text{O} \rightarrow \text{NH}_2\text{OH} + \text{HNO}_3 + \text{H}_2\text{O}$	Activation Energy (kJ/mol) 65.314	Initiation: At anode, $\text{H}_2\text{O}(\text{l}) \rightarrow \frac{1}{2}\text{O}_2 + 2\text{H}^+ + 2\text{e}^-$ $(\text{NH}_3\text{OH})^+\text{NO}_3^- + \text{H}^+ \rightarrow \text{NH}_3\text{OH}^+ + \text{HNO}_3$ At cathode: $2\text{NH}_3\text{OH}^+ + 2\text{e}^- \rightarrow 2\text{NH}_2\text{OH} + \text{H}_2$ Hence, the overall reaction is $\text{H}_2\text{O} + 2(\text{NH}_3\text{OH})^+\text{NO}_3^- \rightarrow 2\text{HNO}_3 + 2\text{NH}_2\text{OH} + \text{H}_2\text{O}$
Ignition: 2. $\text{NH}_2\text{OH} + \text{HNO}_3 \rightarrow \text{HONO} + \text{HNO} + \text{H}_2\text{O}$	30.564	Decomposition: $\text{NH}_2\text{OH} + \text{HNO}_3 \rightarrow \text{HONO} + \text{HNO} + \text{H}_2\text{O}$
Decay: 3. $\text{NH}_2\text{OH} + \text{HONO} \rightarrow \text{N}_2\text{O} + 2\text{H}_2\text{O}$ 4. $\text{NH}_2\text{OH} + \text{HNO} \rightarrow \text{N}_2 + 2\text{H}_2\text{O}$ 5. $3\text{HONO} \rightarrow 2\text{NO} + \text{HNO}_3 + \text{H}_2\text{O}$ 6. $2\text{HNO} \rightarrow \text{N}_2\text{O} + \text{H}_2\text{O}$ 7. $\text{HNO} + \text{HNO}_3 \rightarrow 2\text{HONO}$ 8. $\text{HONO} + \text{HNO}_3 \rightarrow 2\text{NO}_2 + \text{H}_2\text{O}$	14.654 11.723 38.937 72.013 69.920 3.349	Decay: $\text{NH}_2\text{OH} + \text{HONO} \rightarrow \text{N}_2\text{O} + 2\text{H}_2\text{O}$ $\text{NH}_2\text{OH} + \text{HNO} \rightarrow \text{N}_2 + 2\text{H}_2\text{O}$ $3\text{HONO} \rightarrow 2\text{NO} + \text{HNO}_3 + \text{H}_2\text{O}$ $2\text{HNO} \rightarrow \text{N}_2\text{O} + \text{H}_2\text{O}$ $\text{HNO} + \text{HNO}_3 \rightarrow 2\text{HONO}$ $\text{HONO} + \text{HNO}_3 \rightarrow 2\text{NO}_2 + \text{H}_2\text{O}$

III. EXPERIMENT

A. Synthesis of HAN solution

HAN solution was prepared by titration between aqueous solution of hydroxylamine (50 wt%) and nitric acid (35 wt%), both of high purity (Sigma-Aldrich). The process was continuously kept in ice water bath to avoid self-decomposition until pH of the solution reached 2.50. The pristine solution was then further purified in a rotary evaporator (Heidolph Laborata 4003) for 19minutes to achieve approximately 73 wt% HAN solution. By using conventional volume and weight measurement method, the density of the HAN solution is 1.524 g/cm³ while viscosity of the solution at room temperature is 9.0 x 10⁻⁴ PaS (LVDV-II Viscometer, Brookfield).

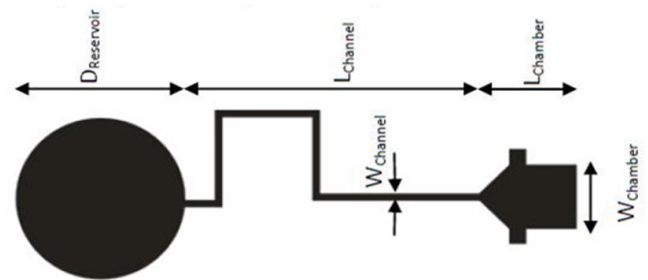
B. Fabrication of micro-combustion

The micro-combustion system consists of a reservoir as shown in the left in Figure 1, a microchannel connecting the reservoir to micro-combustion chamber located at the right of the figure. The design was fabricated using xurographic method, in which the pattern was firstly cut into shape on a vinyl film using a cutting plotter (Graptect CE5000-60), followed by fabrication steps illustrated in Figure 2. After the device was completed, copper wires were directly poked

through the PDMS top layer into the micro-combustion chamber to serve as electrodes, as shown in Figure 3.

Our previous study has shown that macroscale HAN solution decomposition behaviour was influenced by electrodes selection [11]. Sacrificial electrodes such as copper wire may generate more reactive chemical reaction compared to inert electrodes.

Three devices were fabricated to study decomposition phenomenon under different flowrates in each micro-combustion chamber. The positions of copper wire electrodes varied slightly even though best effort was put in to ensure consistency. The distances between electrodes in Devices A, B and C were 1.37mm, 0.42mm and 0.98mm respectively. The distances between electrodes at this scale (<5 mm) has negligible influence on the efficiency of electrolytic decomposition [12].



Micro-combustion system dimension		
Reservoir diameter	5 mm	
Micro-channel	Width	0.225 mm
	Length	15 mm
Microcombustion chamber	Top length	0.6 mm
	Bottom length	2.4 mm
	Width	2 mm
Electrodes	Width	0.3 mm

Figure 1: Device pattern on a vinyl film. The circle at the left of the mask indicates the reservoir (5mm radius x 200 μm (H)), connecting to the micro-combustion chamber (2mm (W) x 3mm (L) x 200 μm (H)) via a serpentine microchannel (225 μm (W) x 15mm (L) x 200 μm (H)), which will avoid HAN solution backflow due to high pressure in the micro-combustion chamber. The extra markers (1 mm (W) x 1mm (L) x 200 μm (H)) next to the chamber were used as mark for insertion of copper wire. Post combustion products were released from the combustion chamber into the ambient in the right.

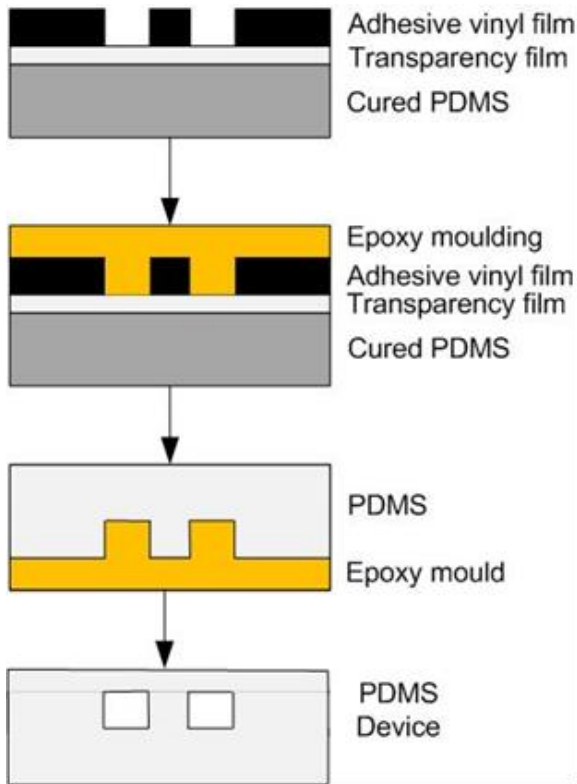


Figure 2: Fabrication of the micro-combustion device. A) The undesired vinyl film was peeled off to create a negative mould attached to a transparent transfer film before it was attached to a PDMS slab to form a mould for the entire microstructure, to encase the poured PDMS mixture. B) Mixture of Bisphenol A (BPA) was poured onto the mould, then cured naturally at room temperature for 48 hours. C) PDMS poured onto the epoxy mold and allowed to dry naturally. D) The channels were formed by sealing it with a PDMS top piece with Piranha solution, followed by thermal curing at 70 °C for 60 minutes [12].

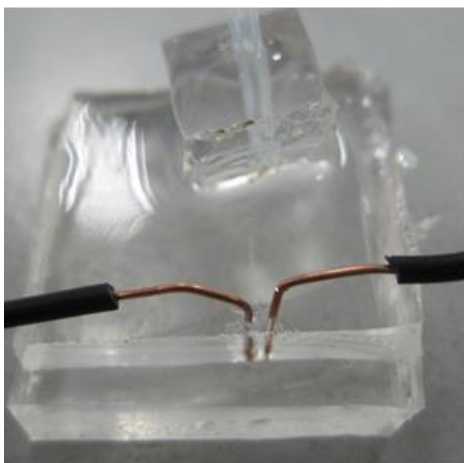


Figure 3: System A with copper wires directly poked into it used as microelectrodes.

Before experiment, the devices were primed with the HAN solution, delivered into the reservoirs through 1/16" PTFE tube (Omnifit) driven by a syringe pump (KDS 210, KDS Scientific), to ensure no air bubbles trapped in the devices. 300W of DC power supply (PS 8040-120 2U, Elektro-Automatik) connected to the copper microelectrodes switched on with the HAN solution continuously fed into the devices. The decomposition lasted for 30 seconds, observed under a light inverted microscope (Olympus IX51) and recorded with a digital camera (Infinity Lite, Lumenera Corp.). The videos taken were processed and splitted into individual pictures (SC Video Cut and Split) for void analysis. Experiment in each device was repeated twice before the bonding finally failed. A video of experiment at $Re = 0.18$ is attached.

Several assumptions were made to facilitate the study. First, the diameter and surface of copper wires were identical in all experiments. Also, all gas bubbles generated in the micro-combustion chambers were only due to decomposition of HAN solution. In addition, in order to facilitate calculation of void fraction in the micro-combustion chamber, gas phase was assumed to be limited by the height of the chamber, like a pancake shape.

IV. RESULTS AND DISCUSSIONS

Figures 4 are series of pictures extracted from videos taken during decomposition of HAN solution in different micro-combustion devices. The dimensions were identical as outlined in green line in Figure 4a. While distance between each pair of electrodes in the devices varied since the copper wires were directly poked into the devices. HAN solution was delivered from upstream reservoir in the left, undergo decomposition in the chamber, followed by displacement into ambient in the right.

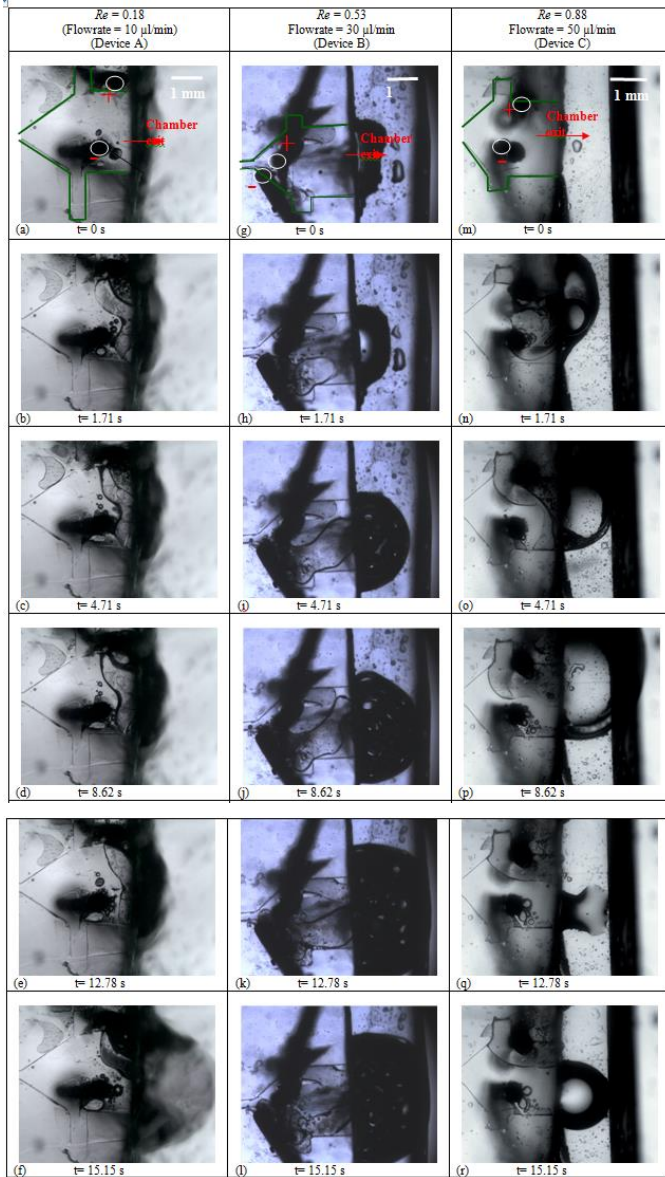


Figure 4: Electrolytic decomposition of HAN solution in different devices using copper wire

When power was switched on (Figure 8b) while Device A was fed with inlet flowrate of $10\mu\text{l}/\text{min}$ or $Re = 0.18$, gas bubbles of oxygen and hydrogen, diameter in the range of $50 - 480\mu\text{m}$ were formed immediately at anode and cathode respectively, with the formation of bubbles at anode was milder than the cathode. Coalescence of bubbles took place before they were displaced to the chamber exit. Wave of decomposition with an interval of 0.92 second was observed with continuous yet consistent full combustion waves with time interval deviation less than 5% was recorded throughout whole experiment (Figure 8b – f).

Low Re preventing gas bubbles displaced to the ambient immediately after decomposition, due to significant wall effect. Some were stagnant almost throughout the decomposition

process, resulted in choking at the exit (Figure 8d – f). The formation of void by trapped gas caused significant problem to the decomposition in the micro-chamber. Increase in void fraction causes increase in electrical resistance between the electrodes, even breakdown of electrical circuit (Figure 8e, f), resulting in decrease of efficiency. However, the circuit can still be completed through HAN solution accumulated at the chamber exit. In this circumstance, small air bubbles continuously formed at the electrodes as decomposition took place in random pattern both spatially and temporally in the chamber. The processes caused the void inside the micro-combustion chamber varied from $38 - 60\%$. Besides, no brownish post-combustion gases were noticed throughout experiment as the decomposition became more vigorous with post-combustion gas propagate to the exit.

In Device B, experiment was repeated at $Re = 0.53$. The decomposition phenomenon could be divided into two main visible stages, i.e. the transient and steady decomposition stage. In the transient stage, vigorous and continuous bubbles formation took place at both electrodes that the interval delay between bubble formation reduced from 0.55s down to 0.31s (Figure 8g) before it moved into the steady stage, in which the decomposition behaved more vigorous and propagated towards the chamber exit as continuous growth in two phases flow from $t = 4.02\text{s}$ until $t = 12.78\text{s}$ (Figure 8i – k). In this stage, time required between bubbles formation at the chamber exit continuously reduced. In addition, gas released from the reaction was significant that occupying $45 - 75\%$ of space in the chamber, causes the wall effect becomes insignificant (Figure 8l). In general, the flow phenomenon in the chamber was more completed with rapid and random formation of large bubbles at the chamber exit.

In Device C, when the flowrate was further increased to $50\mu\text{l}/\text{min}$, at $Re = 0.88$, consistent decomposition interval of 0.5s was noticed for the first 4.5s before the overall process was shortened to 0.2s after a few cycles (Figure 8m – p). The overall decomposition was more rigorous that only few small bubbles formed at the surroundings of electrodes while two phases flow in the chamber is smooth without serious problem of choking the exit. By contrast, space inside the chamber was mostly occupied by gas generated throughout the duration, typically in the range of $58 - 90\%$ (Figure 8p, q). Accumulation of HAN solution in the chamber also shortened significantly because of the relatively high flowrate.

Although flow and chemical reaction phenomenon in the micro-combustion chambers behaved differently as Re increased, no reverse flow into the upstream microchannel was observed in all devices. In addition, the chemical reaction, which was considered highly energetic, caused only slight de-sealing at the surroundings near to the chamber in all devices. However, the devices failed completely after experiments were repeated.

V. CONCLUSIONS

Although PDMS is not the ideal material for constructing micro-combustion system due to its relatively low melting

point, it still enabled visualisation of microscale decomposition of HAN solution, which has never been reported in literature elsewhere. The micro-combustion systems were only effective in relatively high Re in which choking was reduced significantly. In addition, un-decomposed HAN solution in the micro-combustion chambers is the main concern in future engineering design as it caused complex two phase flow which is difficult to predict and reducing efficiency of the devices. The experiment also shows the design is suitable for the decomposition of HAN solution as backflow successfully prevented. Qualitatively, relatively high Re and power required for decomposition of HAN solution to prevent formation of complex two-phase flow in the chamber.

A HAN-based micropropulsion system is currently being developed based on previous micro-combustion system design, by adding a nozzle to the chamber exit. Experiments and Quantitative analysis on various factors, such as packaging of microelectrodes, structural construction material and delivery of HAN solution are also being investigated to increase its efficiency. In addition, numerical studies will also be carried out to improve the engineering design. It is a challenging task as it involves parallel chemical reactions as well as complex liquid-gas two phase flow.

ACKNOWLEDGMENT

The authors would like to thank to Ministry of Science, Technology, and Innovation Malaysia (MOSTI) for funding the project (04-05-05-SF0008) through eScience Fund.

REFERENCES

- [1] N. Klein, Gun Propulsion Technology. In: L. Stiefel, M. Summerfield (Eds.), Progress in Astronautics and Aeronautics, USA 1998, p. 473
- [2] K. Ramohalli, W. Dowler, Helping HAN for hybrid Rockets, Aerospace America 1995, 33, 20-21
- [3] C. Kappenstein, Y. Batonneau, E.A. Perianu, N. Wingborg, Non Toxic as Hydrazine Substitutes Comparison of Physico-chemical Properties and Evaluation of AND and HAN 2nd Conference on Green Propellant for Space Propulsion, Chia Laguna, Sardinia, Italy, 7-8 June 2004
- [4] <http://electronicsbus.com/portable-fuel-cell-generator-usb-fuelcell-charger-usb-fuelcell-charger-instant-power/>; assessed Feb. 2012
- [5] [http://electronicsbus.com/renewable-energy-harvesting-system - alternate-nergy-sources-bioelectricity/](http://electronicsbus.com/renewable-energy-harvesting-system-alternate-nergy-sources-bioelectricity/);
- [6] L.D. Ronald, Process for Concentrating Aqueous Solutions of Hydroxylammonium Nitrate, Euro.Pat.402540, O;in Corporation, USA, 1993
- [7] R.H. Comer, Ignition and Combustion of Liquid Monopropellant at High Pressure 16th International Symposium On combustion, Pittsburgh, USA, August 1996
- [8] T.G. Kang, S.W. Kim, Y.H. Cho, High-Impulse, Low-power, Digital Microthruster Using Low Boiling Temperature Liquid Propellant with High Viscosity Fluid Plug, Sensors and Actuator A 2002, 97, 659-664
- [9] D.H. Lewis, S.W. janson, R.B. Cohen, E.K. Antonsson, Digital Micropropulsion, Sensors and Actuator A, 80, 143-154
- [10] D. Plumlee, J. Steciak, A. Moll, Development and Simulation of an Embedded Hydrogen Peroxide Catalyst Chamber in Low-Temperature Co-Fired Ceramics, Int.J.Appl. Ceram. 2007, 4, 406-414
- [11] K. S. Koh, J.K. Chin, T. F. Wahida, Role of Electrodes in Ambient Electrolytic Decomposition of Hydroxylammonium Nitrate (HAN) Solution, J. Chem. Eng. Data, (Under Review), 2013
- [12] N. Nagai, M. Takeuchi, T. Kimura, T. Oka, Existence of Optimum Space Between Electrodes on Hydrogen Production of Water Electrolysis, Int. J. Hydrogen Energy, Vol 28, pp 35 - 41, 2003